



Published in final edited form as:

IEEE Trans Neural Syst Rehabil Eng. 2013 September ; 21(5): 830–839. doi:10.1109/TNSRE.2013.2259261.

Development of a Multichannel Vestibular Prosthesis Prototype by Modification of a Commercially Available Cochlear Implant

Nicolas S. Valentin, Kristin Hageman, Chenkai Dai, Charles C. Della Santina, and Gene Y. Fridman

Abstract

No adequate treatment exists for individuals who remain disabled by bilateral loss of vestibular (inner ear inertial) sensation despite rehabilitation. We have restored vestibular reflexes using lab-built multichannel vestibular prostheses (MVPs) in animals, but translation to clinical practice may be best accomplished by modification of a commercially available cochlear implant (CI).

We developed software and circuitry to sense head rotation and drive a CI's implanted stimulator (IS) to deliver up to 1Kpulses/s via 9 electrodes implanted near vestibular nerve branches. Studies in two rhesus monkeys using the modified CI (MCI) revealed in vivo performance similar to our existing dedicated MVPs.

Like commercially available CIs, our design uses an external head-worn unit (HWU) that is magnetically coupled across the scalp to the IS. The HWU must remain securely fixed to the skull to faithfully sense head motion with gyroscopes and maintain continuous stimulation. We measured normal and shear force thresholds at which HWU-IS decoupling occurred as a function of scalp thickness and calculated pressure exerted on the scalp. The HWU remained attached across the human scalp thicknesses from 3mm to 7.8mm for forces experienced during routine daily activities, with magnets exerting pressure on the scalp that remains below capillary perfusion pressure.

Keywords

Electrical stimulation; cochlear implant; neural; prosthesis; bilateral vestibular hypofunction

I. INTRODUCTION

The vestibular labyrinth helps maintain gaze and postural stability by driving reflexive eye and body movements in response to head motion. Rotational head motion is normally encoded into vestibular nerve activity by 6 semicircular canals (SCCs), 3 in each inner ear, which modulate afferent neuron firing rates. Damage to sensory hair cells in the SCCs can occur due to infection, Ménière's disease or ototoxic medications, causing impairment of vestibular reflexes. The resulting disequilibrium, blurred vision during head movements, and postural instability degrade quality of life and increase risk of injury due to falls [4].

There is currently no adequate treatment for individuals with bilateral vestibular hypofunction (BVH) who fail to improve despite vestibular rehabilitation exercises. Preclinical studies in rodents and non-human primates strongly suggest that a multichannel vestibular prosthesis (MVP) could improve quality of life for such patients [5-12].

Initial attempts at prosthetic vestibular stimulation in humans using cochlear implant (CI) stimulators have revealed promising preliminary results [13-16]. These stimulation experiments confirmed that in principle, a CI could be used for delivering information to the vestibular nerve. A more complete system design that would adapt a commercial CI to function as a vestibular prosthesis could expedite translating research findings into clinical use by overcoming significant technological and regulatory hurdles.

We adapted a commercially available CI to function as a semi-implantable MVP. Our design includes motion sensors and a power source coupled magnetically to a modified CI's implanted stimulator (IS). Using a CI to implement a complete vestibular prosthesis presents a unique challenge. Unlike a CI, an MVP uses gyroscopes to accurately sense skull rotation in 3D. Consequently, transcutaneous magnetic (mechanical) coupling between the external head-worn component that contains the gyroscopes and the magnetically coupled implant must withstand head movements encountered during normal daily activities (e.g. walking, jogging, climbing stairs), which can include head rotations with peak velocities up to $\sim 400^\circ/\text{s}$ and accelerations up to $\sim 11,500^\circ/\text{s}^2$ (although the vast majority of head movements are much slower) [17]. At the same time, forces on the intervening scalp must not exceed the safety criteria indicated by the capillary perfusion pressure.

We describe our design of the modified CI (MCI), system bench tests and animal experiments, and we examine the technical challenge of maintaining a safe but strong transcutaneous magnetic coupling between the head-worn unit (HWU) and the IS.

II. DEVICE DESCRIPTION

A. System Overview

As shown in Fig. 1, the MCI prototype comprises three main components: a belt-worn unit (BWU), an external head-worn unit (HWU) and an IS. The BWU provides power to the HWU and reads head motion information from gyroscopes and linear accelerometers in the HWU via I2C. Based on the gyroscope measurements, the BWU determines the instantaneous stimulation pulse-rate for each electrode, schedules and sends a command to the HWU to deliver each pulse. The HWU relays the pulse information via the radio frequency (RF) link to the IS. IS in turn delivers each specified electrical current pulse to the vestibular nerve via one of the 9 electrodes implanted in the labyrinth. Under normal operating conditions, the MCI draws 21.1mA from a regulated 3.3V supply.

B. Belt-Worn Unit

The BWU holds two 3.6V lithium-ion AAA-size batteries in parallel (in case one loses charge or is removed), which continuously power the whole MCI for up to 11 hrs via a 3.3V linear regulator. BWU circuitry comprises surface-mount components on one side of a 2-layer $35 \times 49 \times 1.5\text{mm}^3$ printed circuit board (PCB). A $9 \times 9 \times 1\text{mm}^3$ mixed-signal

microcontroller (μC ; MSP430F1611, Texas Instruments, Dallas, TX), running at 8MHz, controls the system. Using a second timer running at 32.768KHz, the μC samples gyroscope in the HWU every 5ms ($f_s=200\text{Hz}$) and controls stimulus pulse timing. A Bluetooth module (RN-42, Roving Networks, Los Gatos, CA) facilitates parameter changes for patient fitting. This small ($13\times 26\times 2\text{mm}^3$) low power device provides wireless communication at up to 3Mbps, enabling subjects to move within 20m of a fitting computer while parameters are adjusted. All components are encased in a plastic housing for protection and easy attachment to the patient's belt. Including batteries, the whole BWU weighs $\sim 49\text{g}$.

C. Head-Worn Unit

HWU circuitry occupies both sides of a 4-layer $18\times 15\times 1.5\text{mm}^3$ PCB including a 'slave' μC (MSP430F1611) that receives commands from the BWU via I2C and relays them to the IS via the CI's RF link, a surface-mount tri-axial ITG-3200 gyroscope (InvenSense, Sunnyvale, CA) for angular velocity measurement, and a ADXL345 tri-axial linear accelerometer (Analog Devices, Norwood, MA). Accelerometer is included in the design to accurately measure the HWU's orientation relative to the skull during the fitting sessions. These measurements would in turn allow the real time software to compensate for misalignment between SCC's and the HWU's gyroscope axes.

HWU components are encased in a plastic housing coupled magnetically across the scalp to the IS via 3 replaceable magnets arranged to align with magnets on the IS, positioning the HWU so that gyroscope axes approximately align with the SCC axes. The HWU weighs $\sim 10\text{g}$ without magnets and $\sim 18\text{g}$ with the heaviest magnets.

D. Internal Stimulator

The MCI uses a modified 'Concerto' IS (Med-El Elektromedizinische Gerate GmbH, Innsbruck, Austria). Its $25\times 17\times 4.5\text{mm}^3$ hermetic housing, inductive coil, 12 feedthroughs and internal circuitry remain unchanged. However, two alterations were made.

The first modification replaces the standard CI electrode array with a new array designed for stimulation of the vestibular nerve. The electrode array design was developed for non-human primate studies for use with the MVP [18]. In brief, an array of 9 active and 2 reference 90/10 Pt/Ir electrode contacts is embedded within two silicone carriers. The design is based on anatomic measurements from 3D reconstructions of macaque temporal bones. A dual fork-shaped array facilitates placement into the horizontal and superior SCC ampullae, while a second array facilitates placement into the posterior SCC ampulla. The reference electrode can be positioned either in the temporalis muscle or in the perilymphatic space of the common crus within the labyrinth.

The second modification is the addition of magnets for enhanced internal-external device coupling. The need for accurate head velocity measurements and continuous stimulation requires no slippage or rotation of the HWU relative to the IS. Two implantable medical grade magnets (VORP, Med-El Corp.) were added to the periphery of the Concerto's magnetic coil, in a triangular configuration with an existing central Concerto magnet (Fig. 2A). The polarity of one magnet is reversed to ensure correct placement.

E. Software

Software controlling MCI function is written in C and conveyed to the μ Cs via a JTAG interface. In the BWU μ C, a main program runs continuously in a low power mode with periodic interruptions by one of two timer-driven interrupt service routines (ISRs): (1) a sensor sample (SS) ISR, which samples the gyroscopes at 200 Hz, and (2) a pulse command delivery (PCD) ISR, which sends pulse commands to the HWU μ C at the moment when a pulse must be delivered. One pulse command—two 8-bit words specifying pulse width (PW), stimulation channel, and current amplitude—is sent for each stimulation pulse.

The SS ISR uses a 16-bit continuous counter driven by a 32.768KHz sub-main clock (SMCLK) to interrupt the main program every 5ms and read the digital output from the sensors. Obtaining the three measurement values for each rotation axis from the gyroscope once takes 231 μ s. As soon as the values are stored, the BWU μ C immediately returns to the main program.

When new gyroscope samples are available, the main program updates stimulation pulse rates by calculating the 'time-until-next-pulse' (TUNP) for each channel (taking 180 μ s per channel), as described in detail by Chiang et al 2011 [18]. Briefly, angular head velocities obtained from the gyros in $^{\circ}/s$ are converted into instantaneous pulse frequencies using a 32-point piecewise-linear approximation to a sigmoid curve, where gyro input ranges from 0 (corresponding to 500 $^{\circ}/s$ head rotation toward the implanted labyrinth) to 4095 (500 $^{\circ}/s$ away), with 2048 corresponding to zero head velocity. A 32 bin look-up table of slopes and intercepts facilitates efficient calculation of this nonlinear mapping function in a compromise between computational time and memory use. After scheduling the pulses the BWU μ C enters sleep mode again.

The PCD ISR interrupts the main program whenever a stimulation channel's TUNP timer reaches zero, and sends a pulse command, one 8-bit word at a time with parity checking, to the HWU μ C via I2C. Occasionally, the asynchronous PCD routine for a given channel must wait briefly until another channel finishes delivering a pulse command, or until the sensors are sampled, before executing.

F. External Circuitry Housing

Housings were prototyped for both external circuits, as shown in Fig. 2. Designs were developed in SketchUp (Google, Mountain View, CA) and fabricated using a 3D printer via layered acrylonitrile butadiene styrene plastic deposition. The 45 \times 31 \times 10mm³ HWU housing shown in Fig. 2B and 2C accommodates circuitry, an RF coil and three medical grade magnets chosen to accommodate the user's scalp thickness. Magnets are angled inward to fit the radius of curvature of the average adult human skull's scalp near the asterion - 7.8 ± 0.7 cm, measured using a dataset of human head CAT scans (unpublished data). A CAD drawing of the outer aspect of the HWU is shown in Fig. 2C to emphasize the curvature of the device, which is otherwise difficult to observe in a photograph. This side of the HWU's housing is coated with silicone (A-103 Elastomer, Factor II Inc., Lakeside, AZ) to increase friction. A 53 \times 47 \times 27mm³ protective housing was similarly designed and manufactured to encase the BWU battery pack and circuitry (Fig. 2D and 2E).

III. MATERIALS AND METHODS

A. External System Performance Tests

1) Gyroscope Modulation—Bench-top performance tests were completed to assess the external component's ability to sense head angular velocity and modulate pulse rate. Pulse command signals were observed simultaneously on all channel outputs from the HWU as it rotated sinusoidally on a servo-controlled earth-vertical-axis rotator at 1Hz with 50°/s peak velocity about the roll, pitch, and yaw axes. Then to test communication reliability, pulse command transmission and reception between BWU and HWU were tested continuously for 24 hr at 400 commands/s over a 98cm cable. The cable was positioned adjacent to unrelated CI head-worn components placed on the test bench to generate RF noise. Since one command is sent for each pulse delivered, we monitored the command and stimulus pulse rates to test for transmission errors.

2) Magnetic Retention Forces and Pressure—Proper MCI function requires the HWU to remain securely coupled to the IS across the scalp to both transduce head motion accurately and maintain power and signal transmission. While fixation could be accomplished using percutaneous posts implanted in the skull, that approach allows a path around the post for transit of infection. We therefore sought to determine whether coupling could be achieved using high-field rare-earth medical grade magnets such that retention forces are sufficient to maintain coupling during daily activities without preventing capillary perfusion.

Threshold decoupling forces were measured across the scalp of a human cadaver temporal bone (TB) specimen and the pressure exerted on the scalp was calculated. Tissue thickness was measured at each magnet site. A post-auricular incision was made, the modified IS was implanted, and the incision was sutured closed. The HWU was then magnetically attached across the scalp, and threshold decoupling forces were measured by pulling in the superior, anterior, inferior, and outward directions with a digital hanging scale (SR-1 1000g × 1g, American Weigh Scales Inc., Norcross, GA). Five measurements were made in each direction using each of six combinations of different magnets—MedEl Amade #3, #4, and #5, with residual flux densities of 1.17, 1.33, and 1.39 Tesla respectively. The strongest magnet was always placed in the center position (Fig. 2).

Lack of TB specimens uniformly spanning the range of typical human adult scalp thicknesses (90/10-percentile is from 3.5–8mm [19]) prompted us to use a synthetic material to simulate scalp tissue in subsequent measurements. Preliminary investigation showed the texture and consistency of cork would provide an adequate approximation to scalp tissue. Thin cork pads were stacked and attached to a plastic human skull model, and force and pressure measurements were obtained in the same manner as with the TB specimen.

B. Internal System Performance Tests

To verify functionality of the internal system, we used the Pulsar IS (Med-El), a ceramic encased IS that functions in the same way as the Concerto IS (which replaced the Pulsar in later design iterations). The IS was controlled via a Research Interface Box II (RIB II;

Leopold-Franzens-University of Innsbruck, Austria [20]) (Fig. 3). We used this separate setup to test the internal system performance due to proprietary restrictions on the RF design associated with the Med-El hardware.

1) Current Amplitude Measurements—Prior to animal testing, the current delivered by the Pulsar and by our lab-built MVP2 were measured on a test-bench using a sense resistor wired in series with a Teflon-coated steel wire (Cooner Wire, Chatsworth, CA) submerged in 0.9% NaCl saline.

2) In vivo Physiological Studies—Studies were performed on two rhesus monkeys (F20124RhB and F060738RhG, referred to as monkey A and monkey B respectively; *Macaca mulatta*; 5-12 kg) under a protocol approved by the Johns Hopkins Animal Care and Use Committee, which is accredited by the Association for the Assessment and Accreditation of Laboratory Animal Care, and consistent with European Community Directive 86/609/EEC. The purpose of these experiments was to test if the MCI can deliver stimulation pulse trains evoking responses similar to those elicited with the MVP2.

a) Surgery: Each animal was implanted with (1) an acrylic head cap surgically affixed to the skull to aid in stereotaxic placement during experiments, (2) two scleral coils for 3D measurement of eye movements, and (3) an array of electrodes inserted into the left ampullae. Vestibular function was ablated via intratympanic injection of gentamicin. Procedures were performed under sterile conditions and 1.5-5% isoflurane anesthesia.

Surgical methods of head-cap, scleral coil, and electrode implantation have been previously described [18, 21-23]. In brief, a light poly-ether-ether-ketone head cap was first affixed to the animal's skull using titanium bone screws. Then, two polytetrafluoro-ethylene-coated steel wire (Cooner Wire, Chatsworth, CA) search coils were sutured to the sclera of each eye—one around the iris and another roughly orthogonal to the first—and wires were run to the connectors within the head cap. In a separate surgical session, electrodes were implanted into the left labyrinth. First, a mastoidectomy was performed, followed by exposure of the SCCs, each of which was then opened near the junction of the thin segment and the ampulla. The forked electrode array was inserted near the junction of the superior and horizontal SCCs, and the single-tine array was inserted into the posterior SCC. Additional reference electrodes were inserted in the labyrinth and beneath the temporalis muscle [21, 24]. Electrode leads were then run under periosteum and terminated in a connector on the head cap so our MVP2 or MCI connector could be attached.

After recovery from implantation, intratympanic gentamicin was administered using a standard clinical dosing regimen similar to the one used in humans [25]. During each treatment, ~0.5mL of 26.7mg/mL buffered gentamicin solution was injected through the ear drum into the middle ear, resulting in ablation of labyrinthine mechano-sensitivity. Treatments were repeated every three weeks until vestibulo-ocular reflex (VOR) responses to ipsilateral head rotations had <10% of normal gain. In each case, 2-3 injections per ear were required.

b) Stimulation Paradigm: VOR responses were elicited using the Pulsar and our MVP2 to present frequency-modulated, charge-balanced, cathodic-first (at the SCC electrode), 150 μ s per phase, biphasic pulse stimuli, similar to those used in our previous primate experiments with the dedicated MVP2 [26]. To ensure evoked responses were due solely to prosthetic stimulation, animals were kept stationary (no head or body rotation/translation) and gyroscope signals were replaced with software controlled digital signals representing virtual head rotations. Stimulation pulse timing was calculated by a computer, which passed pulse command signals determining pulse timing, PW, current amplitude and active electrode to the Pulsar via the RIB II's RF link.

Before starting each experiment, electrode currents were optimized by defining thresholds and maximal levels at which signs of current spread occur, and setting constant amplitudes to 10% below the maximum level. Current was slowly increased while sinusoidal pulse rate modulation corresponding to virtual 1Hz, 50°/s head movement was delivered to the electrodes (see the mapping between head velocity and pulse rate description below). Threshold current was determined to be the current amplitude at which eye movements of ~10°/s were observed, and maximum current was determined to be just below the current that elicited large eye movement axis changes or visible facial muscle responses (both indicating unacceptable current spread). Stimulation thresholds vary between SCCs and between animals, so different current amplitudes were used for each SCC, ranging from 100-200 μ A.

Once currents were optimized, the animal was stimulated at the 96 pulses-per-second (pps) baseline rate until the frequency of nystagmus – fast reflexive eye movements due to asymmetric input from the two vestibular labyrinths – fell to <1 per 30s of observation. This took ~5 min. Then, stimuli based on a previously described velocity-to-frequency map designed to emulate normal behavior of rhesus vestibular primary afferents ($f_{base}=96pps$, $f_{max}=350pps$, $C=2$; based on [27]) were delivered, modulated by virtual sinusoidal head rotations at 0.1, 0.2, 0.5, 1, 2, and 5Hz with 50, 100, and 200°/s peak velocities. This set of 18 different stimulus pulse patterns was presented to each SCC with the animal in complete darkness to ensure the VOR was not suppressed by visual input. Modulated stimuli were given to one SCC at a time (while stimulating the other two at a constant baseline rate), first with the MVP2 and then with the MCI. Each stimulus pulse pattern was given for 10-20 sinusoidal cycles, depending on the stimulus frequency, returning to baseline stimulation for 5s between each set. An LED placed directly in front of the monkey's face was flashed to re-center gaze before each pulse pattern.

c) Eye movement recording: The system used to measure 3D angular eye position has been previously described in detail [21]. In short, the monkey was seated in a plastic chair restrained by the skull cap and secured to the rotator. Three pairs of field coils were attached to the superstructure, generating three fields orthogonal to each other and aligned with the X (nasooccipital, +nasal), Y (interaural, +left), and Z (superoinferior, +superior) head coordinate axes. The X, Y and Z field signals induced across each scleral coil were demodulated, filtered, and analyzed using 3D rotational kinematic methods [23, 28]. Angular rotations were expressed as rotation vectors with roll, pitch, and yaw coordinates,

and angular velocity vectors of eye with respect to head were calculated from the corresponding rotation vectors [29-31].

d) Eye Movement Analysis: Eye movement data analysis methods have been previously described in detail [7]. Briefly, data were analyzed using a custom software package written in LabVIEW that incorporates 3D rotational kinematics [32]. The eye movements were calculated in the reference frame corresponding to the SCC axes: the left-anterior/right-posterior axis (LARP), the right-anterior/left-posterior axis (RALP), and the horizontal axis. 3D Eye rotation velocity was calculated from linearly interpolated and filtered eye movement data. Peak eye velocity was calculated for each cycle-averaged pulse train. Trials in which the monkey blinked or fell asleep were disregarded. Aggregate values are reported as mean \pm sample standard deviation.

IV. RESULTS

A. External System Performance

1) Gyroscope Modulation—Instantaneous pulse frequency traces from each output channel (Fig. 4) confirm the external system's ability to modulate pulse rate based on real-time sensor input. During yaw rotations, only pulse rate on the horizontal (z) channel modulated. Pitch rotations elicited anti-phase modulation of the LARP and RALP channels, while roll rotations elicited in-phase modulation.

No errors resulted from continuous pulse command transmission and reception between the BWU and HWU over 24 hr at a rate of 400 commands/sec, indicating that cable length and close proximity to active RF hardware does not affect I2C communication.

2) Magnetic Retention Forces and Pressure—Fig. 5 shows force measurements taken using various combinations of external magnets. During routine daily activities, based on the maximum HWU weight of 17.56g, the HWU would experience the greatest anterior/tangential and inferior/tangential forces (222 ± 40 and 474 ± 71 mN respectively) while jogging (j) and the greatest outward/centrifugal force (3 ± 2 mN) while climbing down stairs (s). In extreme cases, vigorous voluntary yaw rotations (v) can reach average peak velocities of $\sim 780^\circ/\text{s}$ (ranging from 380 - $1100^\circ/\text{s}$) [33] and the HWU can experience average outward/centrifugal forces of ~ 253 mN. However, such high velocities are not reached during routine head movements. It is worth noting that outward forces due to walking, jogging, and climbing stairs are $\leq 1.2\%$ of the force experienced during voluntary yaw rotations and they are too small to be seen in Fig. 5C. In the anterior and outward directions (Fig. 5A and 5C) decoupling thresholds with all magnet combinations across all tissue thicknesses were $\geq 181.9\%$ of the mean anterior and outward forces expected for the HWU during jogging in Fig. 5A, and vigorous voluntary yaw rotations in Fig. 5C. In the inferior direction (Fig. 5B), not all magnet combinations provided sufficient retention force across all tissue thicknesses. For 6mm and thinner tissue, decoupling thresholds for all combinations were $\geq 150.3\%$ of the mean jogging decoupling forces. For 7.8mm tissue, however, combinations 1–4 were marginal at $\geq 101\%$, while combinations 5 and 6 yielded $\leq 92\%$ of the forces, meaning that the HWU could fall off in those circumstances. Similarly, for 9mm tissue, all thresholds were $\leq 81\%$ of the mean jogging decoupling forces.

Fig. 5C (right side axis) shows pressure exerted by HWU-IS coupling on the intervening tissue using different magnet combinations. No single definitive capillary blood pressure value was found in literature and the measurements presented by multiple sources are shown in the plot. Here we use the most commonly accepted mean capillary pressure (MCP) measurements reported by Landis (indicated with a black dot along the right axis, MCP = 22mmHg) [1] as our benchmark criteria. For scalp thickness ≥ 7 mm, pressure exerted by all magnet combinations was below the MCP. For 3mm, magnet combinations 1, 2, and 3 exceeded the MCP at 120%, 110% and 103% of MCP respectively, and combinations 4-6 were below the MCP at ≤ 8 % of MCP.

B. Internal System Performance

1) Current Measurements—Current delivered by each channel was quantified for both the Pulsar and the MVP2. In most cases, actual current delivered was slightly different than expected, yet never below 93% of the expected value. As determined by the area under the biphasic curves, the MCI delivered 99.3% of the charge delivered by the MVP2.

2) In vivo Physiological Experiments—Fig. 6 shows a side-by-side comparison of responses elicited by both prostheses in monkey A, for one cycle of sinusoidal pulse frequency modulated stimulation of each SCC at 1Hz from 68-130pps (equivalent to 50°/s peak velocity in normal animals using the previously referenced velocity-to-frequency sigmoidal map). Standard deviation was less than 3.8°/s for all traces. Fig. 7 shows excitatory and inhibitory amplitude responses elicited in monkey A with both prostheses. Difference in responses evoked with each prosthesis were ≤ 3 °/s for monkey A and ≤ 7 °/s for monkey B across all stimulation frequencies (0.1–5Hz), for all sinusoidally modulated stimuli. Combining data for both monkeys, MVP2 responses ranged from 2.6- 20.1°/s and MCI responses ranged from 2.2-19.8°/s.

V. DISCUSSION

To expedite realization of a vestibular prosthesis for clinical use, we sought to modify the hardware and software of a commercially available CI and to determine whether it could function as an MVP. Our findings indicate that an MCI can be a viable alternative implementation of a vestibular prosthesis.

Size and power: Uninterrupted stimulation and accurate head motion measurement are important for proper function of an MVP, so the HWU must be as small and light as possible to reduce the possibility of accidental decoupling or slippage. HWU size and weight have been minimized by placing components that do not require head fixation or proximity to the IS in the BWU. The inductive power link avoids the need for a percutaneous connection and reduces risk of infection, but it incurs poorer power transmission efficiency. The BWU allows use of a large battery pack to supply the high current demands, and it includes a backup battery to maintain continuous function when a battery must be replaced.

Gyro modulation tests: As expected, slight stimulus asymmetry in pulse rate curves (Fig. 4) is seen for pulse rate above vs. below the 96 °/s baseline. This asymmetry is the result of the

nonlinear sigmoidal relationship between the gyroscope measurements and the corresponding pulse rates computed in the BWU μ C.

Magnetic retention forces and pressure: Although an extensive literature search did not identify a single consensus value for a “safe threshold” external pressure below which scalp perfusion is not compromised, available literature suggests that it is likely to be somewhere in the range of 20–25mmHg. Arteriolar- and venous-end capillary perfusion pressures provide liberal and conservative extremes, but the mean capillary perfusion pressure (e.g., 22 mmHg per the Landis study), seems to have become the consensus criterion for scenarios like the MVP.

Optimal coupling can be achieved using different magnet combinations for scalp tissue ranging from 4.6–7.8mm. For patients with scalp >7.8mm, retention force would not be sufficient to maintain stable coupling through the range of active head movements. Because the coupling pressure was significantly below the MCP for these patients, it would be possible to add extra magnets to establish a more secure coupling without incurring the extra safety risk. For patients with scalp <4.6mm, pressure exerted on the tissue would exceed the MCP for magnet combinations 1, 2, and 3. Because the magnet pressure appears to be only marginally below the MCP for the magnet combinations 4, 5, and 6, magnet strength can be reduced further by placing other non-ferromagnetic material under each magnet in the HWU housing.

The difference between the measurements taken using cork and the TB specimen increased as magnetic force increased. On the TB specimen more force was required to decouple the HWU likely due to the higher compressibility of the scalp which allows the HWU to slightly dimple the tissue and resist greater tangential forces. All measurements taken with the human TB specimen with scalp tissue ~6mm are well fit to the regression lines defined by the cork data, being ≤ 32 mN away from the regression line in each case.

In-vivo stimulation: Data in Fig. 6 and 7 show that the MCI's implantable stimulator evokes responses in rhesus monkeys comparable to those evoked with the MVP2 to partially restore the 3D VOR for head rotations about each SCC axis. However, some nonidealities were seen.

First, LP canal stimulation yielded responses of greater magnitude than the LA or LH canals. This could be due to the LP electrode being closer to its target than other electrodes were to theirs.

Second, an excitatory vs. inhibitory asymmetry was seen in the eye responses in Figures 6 and 7. Asymmetry is an inherent feature of VOR responses driven by a single normal ear [34]. It is more apparent during prosthetic stimulation because pulsatile stimuli cannot depress vestibular nerve primary afferent fibers' firing rates below their spontaneous discharge rates. Stimulation protocols in which subjects are allowed to adapt to supernormal baseline rates during pulse frequency and amplitude ‘co-modulation’ are effective in reducing asymmetry [35]. While we did not explicitly test this stimulation strategy the MCI is fully capable of implementing this protocol.

Lastly, although responses were greater in the plane of the stimulated SCC, spurious stimulation of non-target nerves results in misalignment (i.e. eye movements do not precisely align with the 3D axis of head rotation). This is likely due to current spread. We previously showed that incorporating a pre-compensatory 3D coordinate transformation in the prosthesis can reduce the misalignment [9]. As in the asymmetry problem, while we did not explicitly implement the coordinate transformation protocol in the MCI, there are no barriers in its hardware implementation that would prevent coding of this compensation algorithm in the software.

Future directions: We tested external and internal systems separately and verified their functionality. Efforts to combine both systems into one complete, fully functional MCI are underway. Once this is accomplished, we intend to replicate results obtained with our previous MVPs, implementing novel stimulation protocols and algorithms recently developed by our lab to elicit more symmetric responses and improve misalignment [9, 35]. Results to date suggest that realization of the first human-implantable MVP for treatment of BVH is possible using this approach.

Acknowledgments

This work was supported in part by NIH NIDCD grants R01DC009255 and 1F31DC010099-01A1. The authors gratefully acknowledge contributions of: Andreas Jäger, Roland Hessler and Andreas Hofner (Med-EI Elektro-medizinische Geräte GmbH; modified Concerto CI and associated hardware); Erwin Hochmair and Otto Peter (University of Innsbruck; RIBII); Natan Davidovics, Mehdi Rahman, Bryce Chiang, Bryan Ward, Joong Ho Ahn, and Lani Swarthout (Johns Hopkins; analysis software, MVP2 fabrication, editing and animal care). CDS holds an equity interest in and is CEO of Labyrinth Devices, LLC, a start-up company founded to support commercialization of vestibular prosthesis technology. Terms of this arrangement are managed by the Johns Hopkins University in accordance with its conflict of interest policies._

REFERENCES

1. Landis E. Micro-injection studies of capillary blood pressure in human skin. *Heart*. 1930; 15
2. Steinmetz JA, Langemo DK. Changes in occipital capillary perfusion pressures during coronary artery bypass graft surgery. *Adv Wound Care*. May-Jun;1996 9(3):28–32. 1996. [PubMed: 8716271]
3. Ryan D, Allen V, Murray A. An investigation of interface pressures in low air loss beds. *Int J Clin Pract*. 1997; 51(5):296–8. [PubMed: 9489088]
4. Della Santina CC, Migliaccio AA, Hayden R, Melvin TA, Fridman GY, Chiang B, Davidovics NS, Dai C, Carey JP, Minor LB, Anderson IC, Park H, Lyford-Pike S, Tang S. Current and future management of bilateral loss of vestibular sensation - an update on the Johns Hopkins Multichannel Vestibular Prosthesis Project. *Cochlear Implants Int*. Sep; 2010 11(Suppl 2):2–11. [PubMed: 21756683]
5. Rahman MA, Dai C, Fridman GY, Davidovics NS, Chiang B, Ahn J, Hayden R, Melvin TA, Sun DQ, Hedjoudje A, Della Santina CC. Restoring the 3D vestibulo-ocular reflex via electrical stimulation: the Johns Hopkins multichannel vestibular prosthesis project. *Conf Proc IEEE Eng Med Biol Soc*. 20112011:3142–5. [PubMed: 22255006]
6. Dai C, Fridman GY, Chiang B, Davidovics NS, Melvin TA, Cullen KE, Della Santina CC. Cross-axis adaptation improves 3D vestibulo-ocular reflex alignment during chronic stimulation via a head-mounted multichannel vestibular prosthesis. *Exp Brain Res*. May; 2011 210(3-4):595–606. [PubMed: 21374081]
7. Davidovics NS, Fridman GY, Chiang B, Della Santina CC. Effects of biphasic current pulse frequency, amplitude, duration, and interphase gap on eye movement responses to prosthetic electrical stimulation of the vestibular nerve. *IEEE Trans Neural Syst Rehabil Eng*. Feb; 2011 19(1): 84–94. [PubMed: 20813652]

8. Sun DQ, Rahman MA, Fridman G, Dai C, Chiang B, Della Santina CC. Chronic stimulation of the semicircular canals using a multichannel vestibular prosthesis: effects on locomotion and angular vestibulo-ocular reflex in chinchillas. *Conf Proc IEEE Eng Med Biol Soc.* 2011;2011:3519–23. [PubMed: 22255099]
9. Fridman GY, Davidovics NS, Dai C, Migliaccio AA, Della Santina CC. Vestibulo-ocular reflex responses to a multichannel vestibular prosthesis incorporating a 3D coordinate transformation for correction of misalignment. *J Assoc Res Otolaryngol.* Sep; 2010 11(3):367–81. [PubMed: 20177732]
10. Gong W, Merfeld DM. Prototype neural semicircular canal prosthesis using patterned electrical stimulation. *Ann Biomed Eng.* May; 2000 28(5):572–81. [PubMed: 10925955]
11. Della Santina CC, Migliaccio AA, Patel AH. A multichannel semicircular canal neural prosthesis using electrical stimulation to restore 3-d vestibular sensation. *IEEE Trans Biomed Eng.* Jun; 2007 54(6)(Pt 1):1016–30. [PubMed: 17554821]
12. Della Santina C, Migliaccio A, Patel A. Electrical stimulation to restore vestibular function development of a 3-d vestibular prosthesis. *Conf Proc IEEE Eng Med Biol Soc.* 2005; 7:7380–5. [PubMed: 17281986]
13. Wall C, Kos MI, Guyot JP. Eye movements in response to electric stimulation of the human posterior ampullary nerve. *Ann Otol Rhinol Laryngol.* May; 2007 116(5):369–74. [PubMed: 17561766]
14. Rubinstein, JT.; Phillips, J.; Nai, K.; Ling, L.; Bierer, S.; Jameson, E.; Oxford, T. Clinical, Scientific, and Regulatory Roadmap for a Human Vestibular Implant.. ARO 2011 Midwinter Meeting; Baltimore, MD.
15. Guyot JP, Sigrist A, Pelizzone M, Kos MI. Adaptation to steady-state electrical stimulation of the vestibular system in humans. *Ann Otol Rhinol Laryngol.* Mar; 2011 120(3):143–9. [PubMed: 21510138]
16. Guyot JP, Sigrist A, Pelizzone M, Feigl GC, Kos MI. Eye movements in response to electrical stimulation of the lateral and superior ampullary nerves. *Ann Otol Rhinol Laryngol.* Feb; 2011 120(2):81–7. [PubMed: 21391418]
17. Lasker, D.; Schubert, M. 3-D Measurement of Linear Accelerations and Angular Velocities of the Head, Torso and Leg During Natural Activities. The Association for Research in Otolaryngology, 35th Annual Midwinter Research Meeting; San Diego, CA. 2012;
18. Chiang B, Fridman GY, Dai C, Rahman MA, Della Santina CC. Design and performance of a multichannel vestibular prosthesis that restores semicircular canal sensation in rhesus monkey. *IEEE Trans Neural Syst Rehabil Eng.* Oct; 2011 19(5):588–98. [PubMed: 21859631]
19. Raine CH, Lee CA, Strachan DR, Totten CT, Khan S. Skin flap thickness in cochlear implant patients - a prospective study. *Cochlear Implants Int.* Sep; 2007 8(3):148–57. [PubMed: 17854098]
20. Bahmer A, Peter O, Baumann U. Recording and analysis of electrically evoked compound action potentials (ECAPs) with MED-EL cochlear implants and different artifact reduction strategies in Matlab. *J Neurosci Methods.* Aug; 2010 191(1):66–74. [PubMed: 20558202]
21. Migliaccio AA, Schubert MC, Jiradejvong P, Lasker DM, Clendaniel RA, Minor LB. The three-dimensional vestibulo-ocular reflex evoked by high-acceleration rotations in the squirrel monkey. *Exp Brain Res.* Dec; 2004 159(4):433–46. [PubMed: 15349709]
22. Clendaniel RA, Lasker DM, Minor LB. Horizontal vestibuloocular reflex evoked by high-acceleration rotations in the squirrel monkey. IV. Responses after spectacle-induced adaptation. *J Neurophysiol.* Oct; 2001 86(4):1594–611. [PubMed: 11600623]
23. Robinson DA. A Method of Measuring Eye Movement Using a Scleral Search Coil in a Magnetic Field. *IEEE Trans Biomed Eng.* Oct.1963 10:137–45. [PubMed: 14121113]
24. Dai C, Fridman GY, Della Santina CC. Effects of vestibular prosthesis electrode implantation and stimulation on hearing in rhesus monkeys. *Hear Res.* Jul; 2011 277(1-2):204–10. [PubMed: 21195755]
25. Minor LB. Intratympanic gentamicin for control of vertigo in Meniere's disease: vestibular signs that specify completion of therapy. *Am J Otol.* Mar; 1999 20(2):209–19. [PubMed: 10100525]

26. Dai C, Fridman GY, Davidovics NS, Chiang B, Ahn JH, Della Santina CC. Restoration of 3D vestibular sensation in rhesus monkeys using a multichannel vestibular prosthesis. *Hear Res. Nov*; 2011 281(1-2):74–83. [PubMed: 21888961]
27. Sadeghi SG, Minor LB, Cullen KE. Dynamics of the horizontal vestibuloocular reflex after unilateral labyrinthectomy: response to high frequency, high acceleration, and high velocity rotations. *Exp Brain Res. Nov*; 2006 175(3):471–84. [PubMed: 16957885]
28. Straumann D. [The validity of oculomotor laws]. *Schweiz Arch Neurol Psychiatr.* 1995; 146(4): 151–6.
29. Haslwanter T. Mathematics of three-dimensional eye rotations. *Vision Res. Jun*; 1995 35(12): 1727–39. [PubMed: 7660581]
30. Migliaccio AA, Todd MJ. Real-time rotation vectors. *Australas Phys Eng Sci Med. Jun*; 1999 22(2):73–80. [PubMed: 10474978]
31. Hepp K. On Listing's law. *Commun. Math. Phys.* 1990; 132:285–295.
32. Migliaccio AA, Della Santina CC, Carey JP, Niparko JK, Minor LB. The vestibulo-ocular reflex response to head impulses rarely decreases after cochlear implantation. *Otol Neurotol. Jul*; 2005 26(4):655–60. [PubMed: 16015163]
33. Grossman GE, Leigh RJ, Abel LA, Lanska DJ, Thurston SE. Frequency and velocity of rotational head perturbations during locomotion. *Exp Brain Res.* 1988; 70(3):470–6. [PubMed: 3384048]
34. Ewald, JR. *Physiologische Untersuchungen uber das Endorgan des Nervus Octavus.* Nabu; Wiesbaden, Germany: 1892.
35. Davidovics NS, Fridman GY, Della Santina CC. Co-modulation of stimulus rate and current from elevated baselines expands head motion encoding range of the vestibular prosthesis. *Exp Brain Res.* May; 2012 218(3):389–400. [PubMed: 22349559]

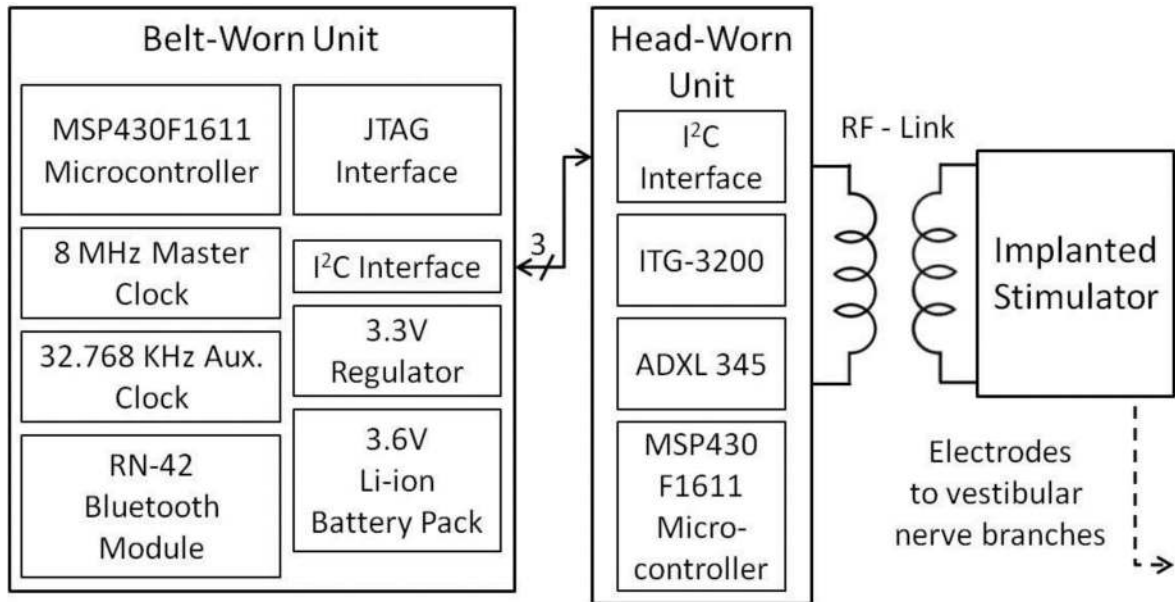


Fig. 1.

Modified cochlear implant circuit block diagram. Our MCI prototype consists of (1) the belt-worn unit (BWU), (2) the head-worn unit (HWU) and (3) the implanted stimulator (IS). The BWU samples sensors on the HWU every 5ms and calculates instantaneous rate of stimulation. Pulse commands are sent to the HWU and relayed via radio frequency to the IS, which delivers frequency-modulated biphasic charge-balanced pulses to the vestibular nerve. Power is provided by a +3.3V supply, drawn from a 3.6V Li-ion battery pack housed in the BWU.

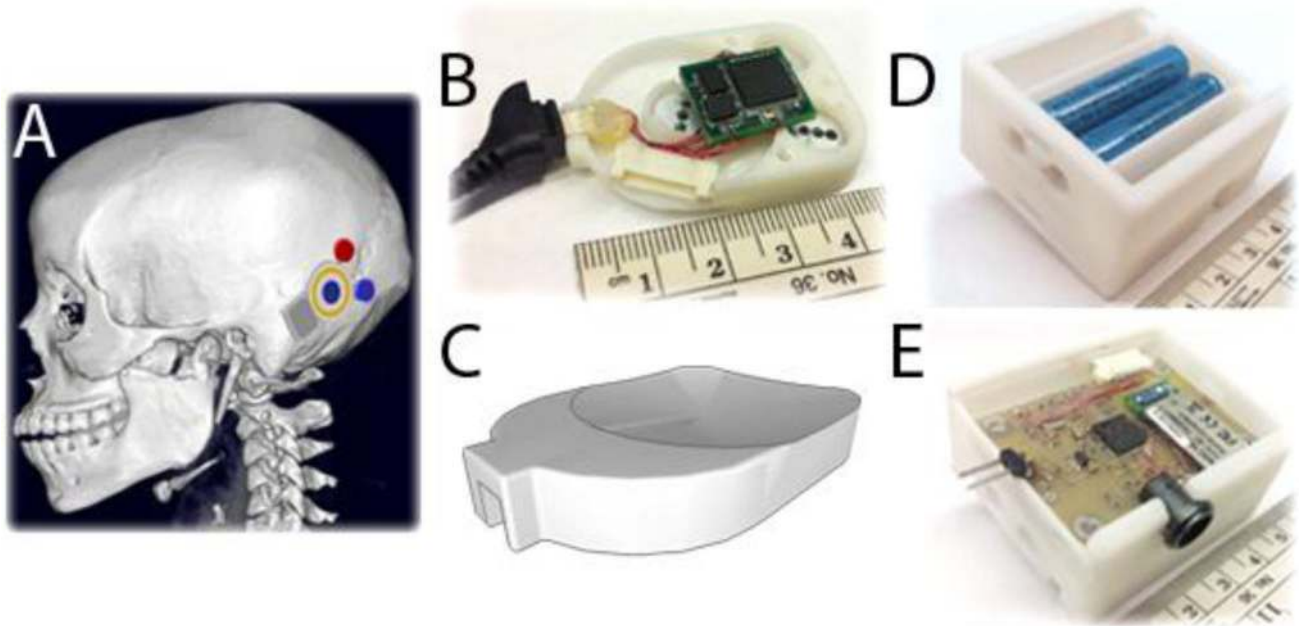


Fig. 2.

(A) The implanted stimulator (IS), which delivers electrical pulses to the vestibular nerve, is shown with supplementary fixation magnets. Its location and position on skull should approximately align gyroscope axes on the head-worn unit (HWU) with each semicircular canal. (B) Top of HWU (without lid) containing circuitry for 3D head motion measurement and pulse command relay to the IS. (C) Bottom of HWU, curved at 7.8cm radius to adapt to the curvature of the average human skull. (D) and (E) show the sides of the BWU (without lids) where batteries and circuitry are held, respectively.

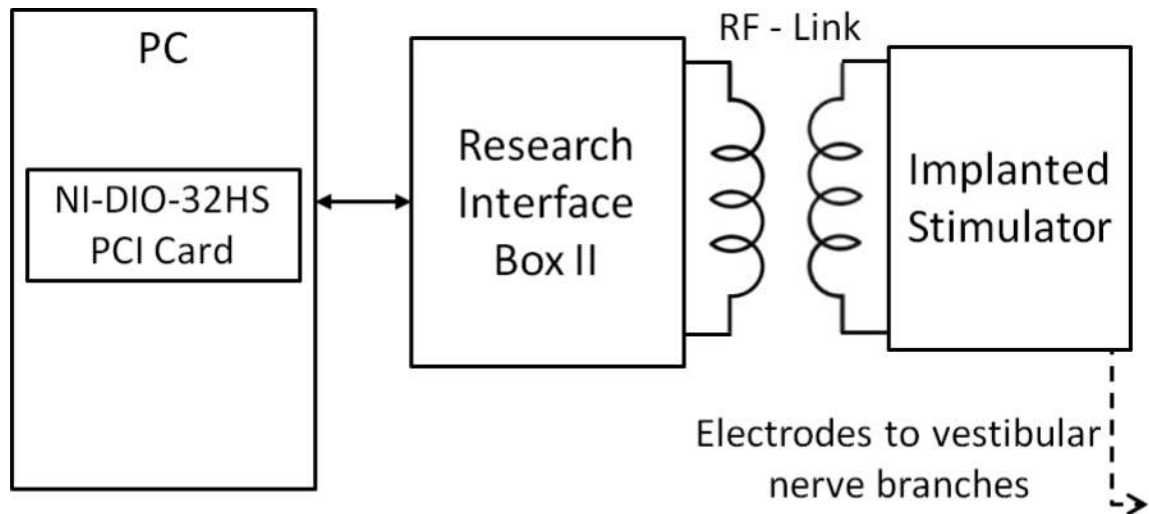


Fig. 3.

Setup used to test performance of the internal system. A computer sinusoidally modulated *virtual* head rotations and calculated timing of pulse commands, which were sent to the implanted stimulator via the research interface box's (RIBII) inductive link. Frequency-modulated biphasic charge-balanced pulses were delivered to each of the monkey's semicircular canals.

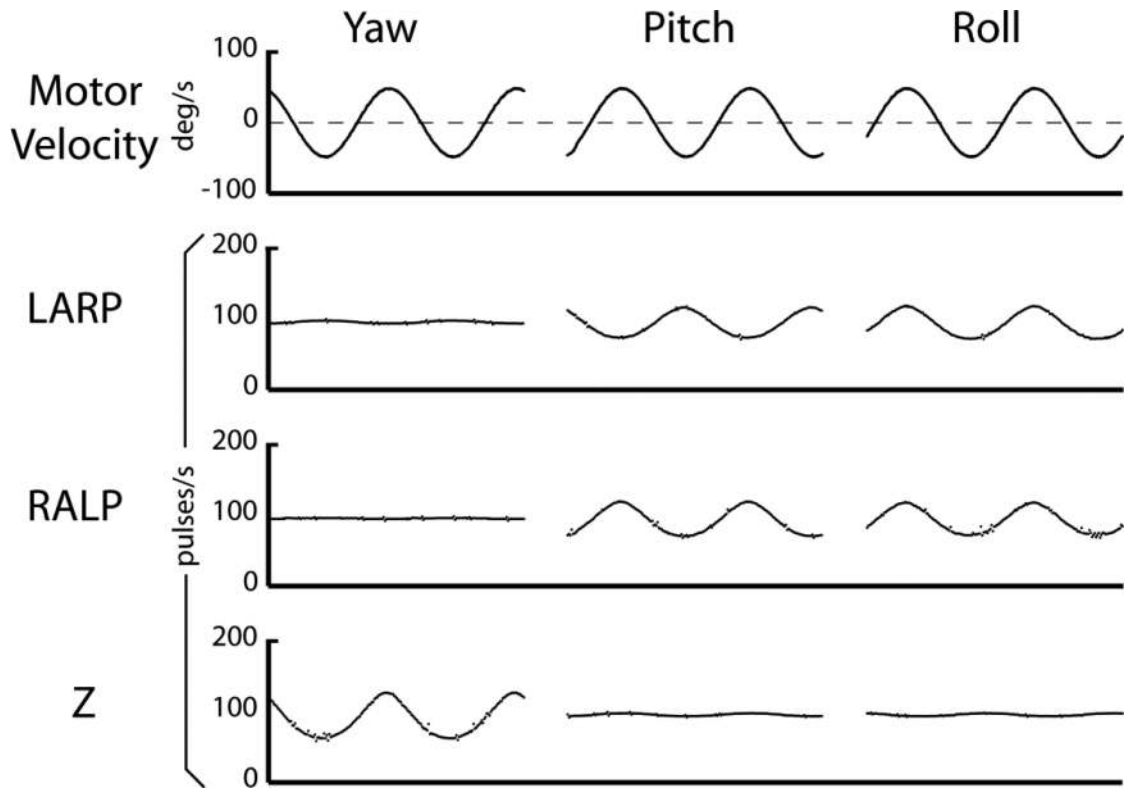


Fig. 4.

Time plots of real-time pulse-command rate modulation by the modified cochlear implant's external system in response to on-axis sinusoidal yaw, pitch, and roll rotations, at 1Hz with a peak velocity of $\pm 50^\circ/\text{s}$. Recordings were taken on three channels concurrently.

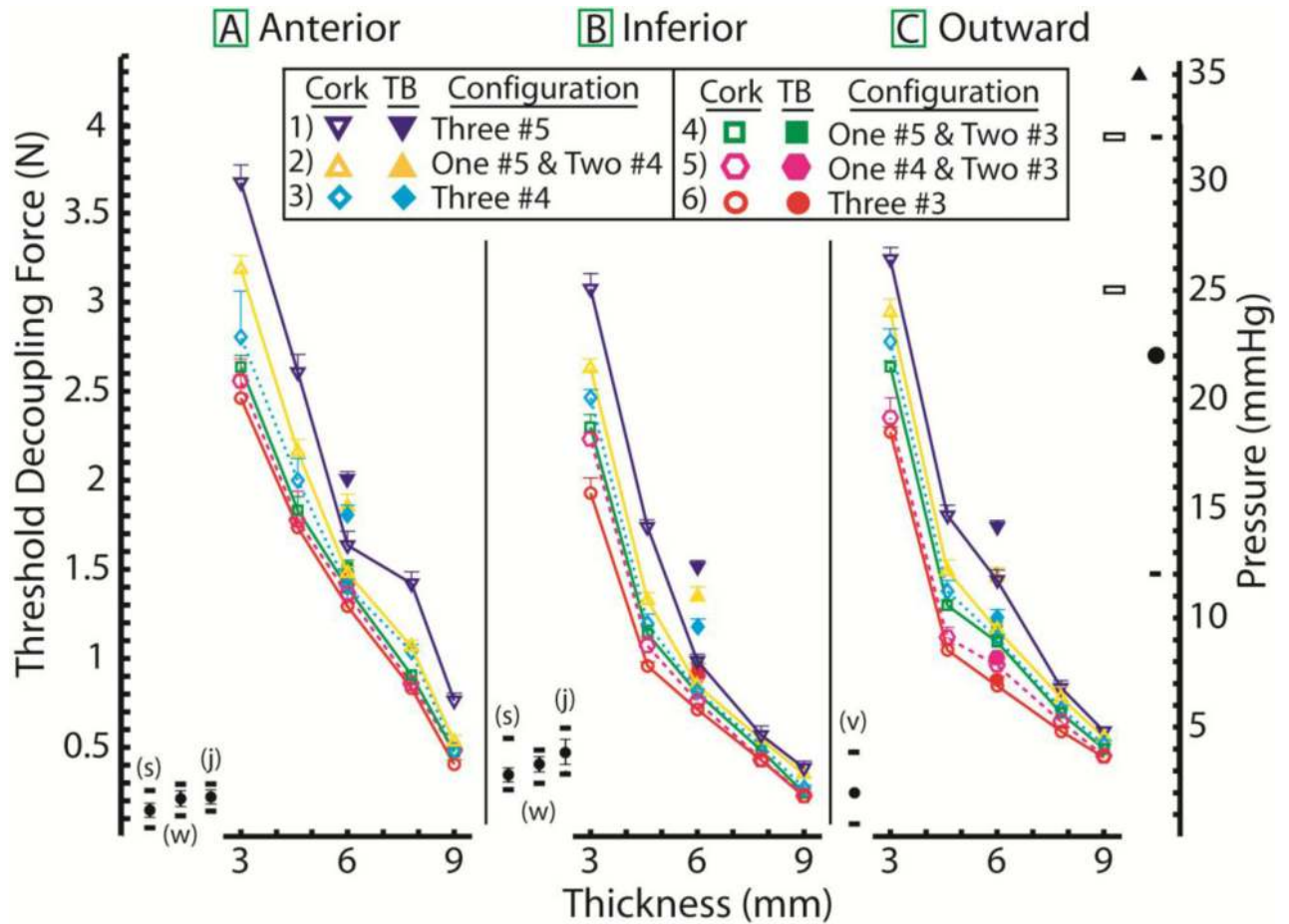


Fig. 5.

The head-worn unit (HWU) was attached to the IS using various magnet combinations across different tissue thicknesses and pulled in the (A) anterior, (B) inferior, and (C) outward directions. Filled and empty shapes denote measurements taken using temporal bone (TB) and cork pads, respectively. Filled circles on left of each plot denote forces on the head during walking (w), jogging (j), climbing stairs (s) and voluntary yaw rotations (v); rectangles denote range. Pressure exerted by all magnet combinations is indicated on the axis at the right of the figure. Mean, arteriolar and venous end pressures according to Landis [1] are denoted by the circle and filled rectangles. Capillary pressure ranges according to Steinmetz and Langemo [2] are denoted by the empty rectangles. Occipital capillary pressure according to Ryan *et al.* [3] is denoted by the filled triangle.

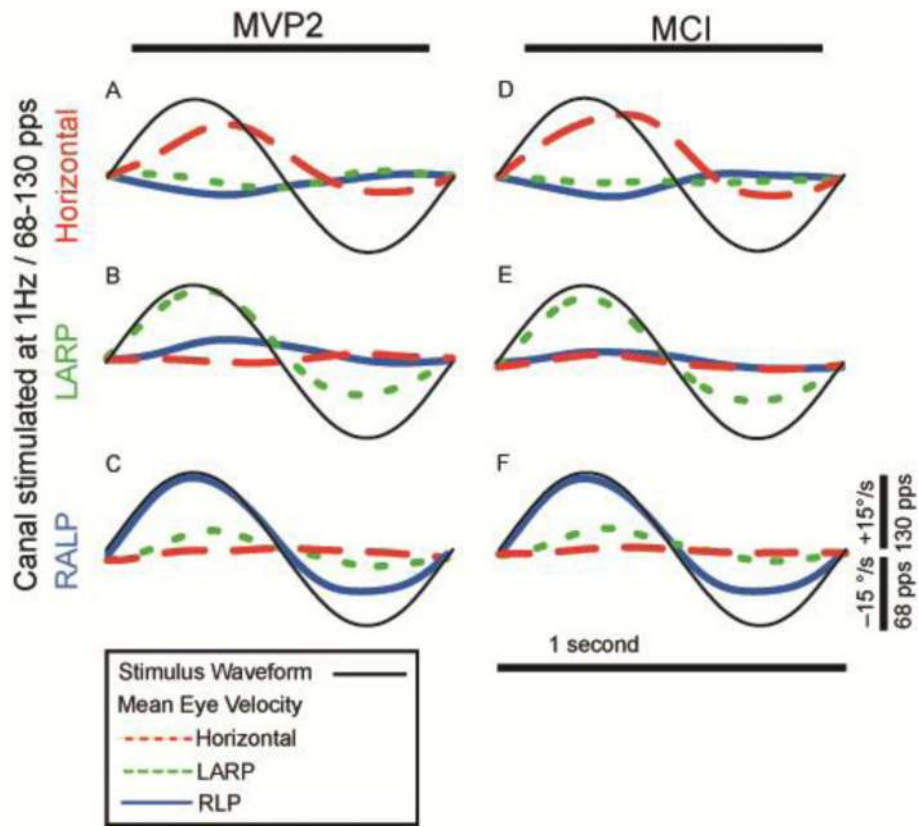


Fig. 6. Comparison of 3D vestibulo-ocular reflex peak responses elicited in rhesus monkey A by delivering stimulation pulses to each canal using our lab-built MVP2 (A-C) and the *Pulsar* IS (D-F). Stimulus was sinusoidally modulated at 1Hz from 68-130pps peak (corresponding $\pm 50^\circ/s$ in a normal animal). Standard deviation was $\leq 3.8^\circ/s$ for all traces.

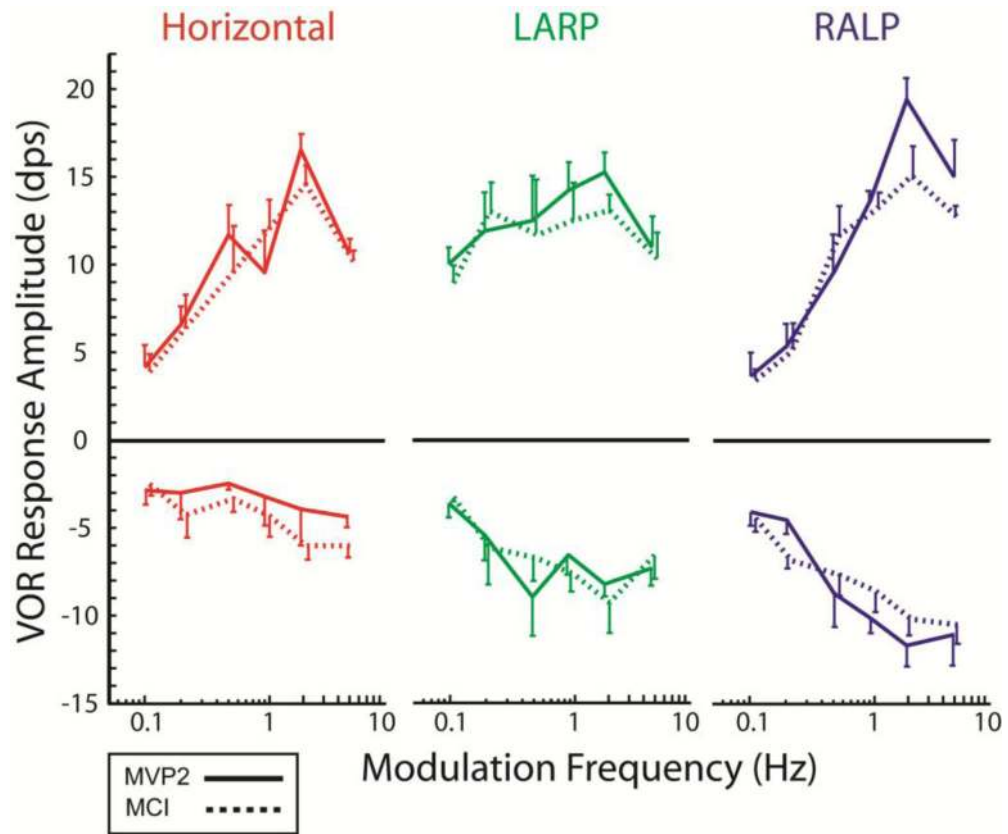


Fig. 7. Excitatory and inhibitory 3D vestibulo-ocular reflex responses elicited in rhesus monkey 'A' by stimulating each left canal using our lab-built MVP2 (solid line) and the MCI (dotted line). Stimulus was modulated at 1-5Hz from 68-130pps peak (equivalent to $\pm 50^\circ/s$ in a normal animal), using the head-velocity to pulse rate mapping curve with $C=2$, baseline pulse rate 96pps, maximum pulse rate 350pps, and current at 150, 170, 200uA for the horizontal, left-anterior, and left-posterior canals, respectively. Mean responses ranged from 2.9-16.5 $^\circ/s$ with the MVP2 and from 2.5-14.6 $^\circ/s$ with the MCI.